Calculation of Wave-Driven Currents in a 3D Mean Flow Model

D.J.R. Walstra[1], J.A. Roelvink[1,2] and J. Groeneweg[1]

Abstract

The theory and implementation of the dominant wave effects in a 3D mean flow model are described. The effects considered are the wave-induced mass flux, wave-induced turbulence, the effects of streaming and forcing due to wave breaking. To model the wave-induced mass flux we have used the GLM method. This method is a hybrid Eulerian-Langrangian approach that also enables the inclusion of a vertically non-uniform mass flux distribution. The model shows good agreement with measurements. It was found that the application of a vertically non-uniform mass flux improves the model predictions considerably. An important conclusion is that with minor modifications any Eulerian-based 2DV, 2DH or 3D flow model can be upgraded to a more physically correct GLM-based model.

Introduction

Within the EU MAST SASME project, a study is being conducted to improve the computed (wave-averaged) currents in nearshore areas in Delft3D-FLOW. Delft3D-FLOW solves the unsteady shallow water equations in two (depth averaged) or three dimensions. In the present version of Delft3D-FLOW the only wave effects that have been included are: a breaking wave-induced shear stress at the surface (Svendsen, 1985 and Stive and Wind, 1986) and an increased bed shear stress (Soulsby et al., 1993). Important wave effects such as the wave-induced mass flux, streaming near the bottom and wave-induced turbulence are not accounted for. In this paper attention is focussed on the incorporation of these wave effects in the 3D mean flow model.

[1] WL | Delft Hydraulics, PO box 177, 2600 MH Delft, The Netherlands.
DirkJan.Walstra@wldelft.nl, Dano.Roelvink@wldelft.nl and Jacco.Groeneweg@wldelft.nl
[2] Delft University of Technology, Department of Civil Engineering and Geo-sciences, Stevinweg 1, 2628 CN Delft, The Netherlands.

Incorporation of wave-induced mass flux

Using the summation convention (Greek indices $\alpha, \beta = 1,2$ corresponding to horizontal coordinates x and y; Latin index $j=1,2,3$ corresponding to x, y, z), the hydrostatic flow equations in Delft3D-FLOW can be written as:

$$\frac{\partial \overline{\zeta}}{\partial t} + \frac{\partial}{\partial x_\beta}\left(\int_{-h}^{\overline{\zeta}} \overline{u}_\beta \, dz + M_\beta \right) = 0, \tag{1.}$$

$$\frac{\partial \overline{u}_\alpha}{\partial t} + \overline{u}_j \frac{\partial \overline{u}_\alpha}{\partial x_j} + g \frac{\partial \overline{\zeta}}{\partial x_\alpha} - \frac{1}{\rho} \frac{\partial \overline{\tau}_{j\alpha}}{\partial x_j} = \frac{F_\alpha}{\rho}, \tag{2.}$$

where $\overline{\zeta}$ is the (short wave) averaged free surface elevation, $\overline{u}$ the horizontal velocity vector, and $\overline{\tau}_{ij}$ shear stress tensor. These quantities are given in a Eulerian (fixed) spatial reference frame. Although Coriolis forces have been taken into account in Delft3D-Flow, they have been omitted here. The influence of the waves is given by the mass flux M and the wave-induced driving force F. The choice of these fluxes strongly affects the mean flow profile, not only in the horizontal direction but also in the vertical direction. However, each formulation encounters the discontinuities at trough level or at the level of the mean free surface. For instance DeVriend and Kitou (1990) mention the difficulties in formulating forces induced by surface waves in a Eulerian framework in a 3D hydrostatic mean flow model. Formulation of the vertical distribution of wave forces in this framework leads to singularities at the mean free surface, due to wave dissipation and wind-input, and at the bottom, due to bottom friction.

In depth-averaged flow equations the mean motion and wave motion are usually separated by averaging over the wave phases (see e.g. Phillips, 1997). However, in the full 3D situation, finding a unique and unambiguous separation of the mean and oscillating motion is difficult in the Eulerian representation of the flow field, because a fixed position at a level between the wave trough and the wave crest is submerged only part of the time. This difficulty can be avoided by considering the Lagrangian representation of the flow field. The simplest idea is Stokes' classical idea of Lagrangian averaging by taking the time mean following a single particle. However, this idea has its limitations since the formulation can not be applied in any exact sense if we wish to speak of the Lagrangian-mean velocity at a given point in space. A followed particle will generally wander away from this point.

In their pioneering paper, Andrews and McIntyre (1978) presented the Generalised Lagrangian Mean theory, or simply GLM. The GLM description is a hybrid Eulerian-Lagrangian description of motion, since it describes the Lagrangian-mean flow by means of equations in Eulerian form with position x and time t as independent variables. Groeneweg and Klopman (1998) and Groeneweg (1999) developed a

GLM-based 1DV and 2DV flow model. Experiences from these studies are used here to formulate the wave-induced effects on the mean flow in Delft3D-FLOW and to interpret the results obtained using this model.

GLM theory. An essential part in the GLM theory is the definition of the particle displacement ξ associated with the wave motion. Like all quantities in the GLM formulation, it is defined as a function of the position x and time t and no longer primarily as a function of the individual particle label as in a purely Lagrangian description. In fact, the generalised Lagrangian flow is described by means of equations in Eulerian form. After having described the disturbance-associated particle displacement field, the exact GLM operator $\overline{(\ )}^L$, corresponding to any given Eulerian-mean operator $\overline{(\ )}$, is defined as:

$$\overline{u(x,t)}^L = \overline{u(x+\xi(x,t),t)} \tag{3.}$$

Eq. (3) implies that the average is taken with respect to the values of u at the disturbed particle positions. In general the combined motion of currents and free-surface waves can be divided into a mean part, an oscillating part and a turbulent part. In Groeneweg (1999), the motion was assumed to be averaged over the turbulent motion. The resulting ensemble-averaged quantities are deterministic and assumed to consist of a mean part and a part representing the wave motion. Groeneweg (1999) only considered periodic, non-breaking waves. By averaging over the short-wave period T, the mean value of an ensemble-averaged quantity u is defined as:

$$\bar{u}(x,t) = \frac{1}{T}\int_{-T/2}^{T/2} u(x,t+t')\,\mathrm{d}t' \tag{4.}$$

This approach implies that interactions between turbulence and wave quantities have been neglected.

In the special case of a slow-modulation average, or more specifically a time average as in Eq. (4), the physical interpretation of the GLM framework is straightforward. Consider the trajectory of a fluid particle starting at point x_0 in Figure 1, i.e. the solution of $\mathrm{d}x/\mathrm{d}t = u(x,t)$. Since u is averaged over the turbulent motion, the trajectory is actually an ensemble-averaged trajectory. In a pure Lagrangian setting the Lagrangian velocity u^L is defined implicitly as:

$$u^L(x_0,t) = u^L\left(x_0 + \int_{t_0}^{t} u^L(x_0,t')\,dt', t\right) \tag{5.}$$

(see e.g. Phillips, 1977), where the velocity of a particle is actually evaluated along its trajectory and assigned to its initial position. The time-averaging process associates two different trajectories with each particle: firstly its actual, rapidly varying trajectory (dashed line in Figure 1) and secondly its mean, slowly varying trajectory (solid line in Figure 1).

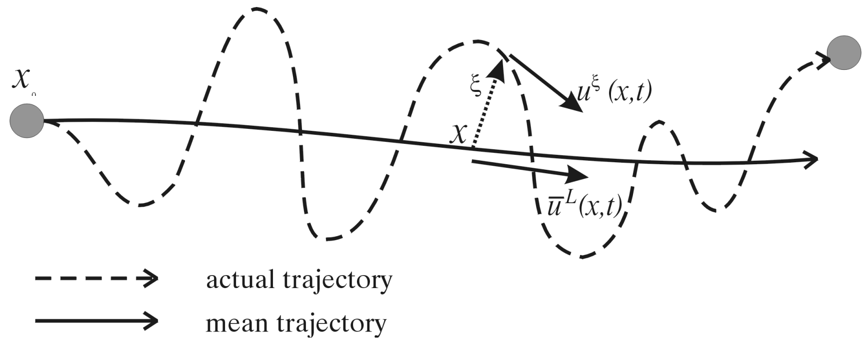

Figure 1. Mean and actual particle trajectories.

The GLM theory claims the existence of a disturbance-associated particle displacement field $\boldsymbol{\xi}$, that links both trajectories (dotted arrow in Figure 1). In the ensemble-averaged setting $\boldsymbol{\xi}$ is fully determined by the wave motion. In the GLM setting a position x at time t is interpreted as a mean position corresponding one to one to an actual particle position $x+\boldsymbol{\xi}$. The actual or generalised Lagrangian velocity is again evaluated at the actual position, but it is now assigned to the mean position:

$$u^{\xi}(x,t) = u\big(x+\xi(x,t),t\big) \qquad (6.)$$

The GLM velocity is defined by taking the time average of Eq. (6), according to Eq. (3). The trajectories of points moving with velocity $\overline{u}^{L}$ are exactly the mean particle trajectories sought. The analogy between Eqs. (5) and (6) reveals the Lagrangian aspects in the GLM method. However, the field x depends on the position x and time t, and is thus no longer primarily a function of the individual particle label, as in a purely Lagrangian description.

GLM flow equations. Andrews and McIntyre (1978) derived the exact GLM equations of motion from the compressible Navier-Stokes equations. Nevertheless, the GLM theory can also be applied to incompressible flow problems, as in Groeneweg and Klopman (1998). The general idea is to consider the quantities in the flow equations for the combined motion of waves and current at their displaced positions and then take the mean of the resulting equations. For an extensive description of the derivation of the GLM equations your are referred to Groeneweg (1999). Only the results of this derivation are presented in this paper.

We start with the Reynolds-averaged Navier-Stokes equations for the total motion:

$$\frac{\partial\zeta}{\partial t}+\frac{\partial}{\partial x_\beta}\left(\int_{-h}^{\zeta}u_\beta\,dz\right)=0 \tag{7.}$$

$$\frac{\partial u_\alpha}{\partial t}+u_j\frac{\partial u_\alpha}{\partial x_j}+\frac{1}{\rho}\frac{\partial p}{\partial x_\alpha}-\frac{1}{\rho}\frac{\partial\tau_{j\alpha}}{\partial x_j}=0 \tag{8.}$$

Note that the quantities in these equations consist of a mean and an oscillating part. By evaluating these equations at disturbed positions and averaging the result over the short wave motion, the GLM flow equations are obtained:

$$\frac{\partial\bar{\zeta}^L}{\partial t}+\frac{\partial}{\partial x_\beta}\left(\int_{-h}^{\bar{\zeta}^L}\bar{u}_\beta^L\,dz\right)=F_c \tag{9.}$$

$$\bar{D}^L\bar{u}_\alpha^L+g\frac{\partial\bar{\zeta}^L}{\partial x_\alpha}-\frac{1}{\rho}\frac{\partial\bar{\tau}_{j\alpha}^L}{\partial x_j}=S_\alpha \tag{10.}$$

The right-hand side F_c of the depth-integrated continuity equation can be expressed entirely in terms of wave quantities. This second-order term (in $/\boldsymbol{\xi}/$, and thus in wave amplitude) is small and is neglected here. $\bar{D}^L=\partial/\partial t+\bar{u}_j^L\partial/\partial x_j$ denotes the rate of change of the GLM flow. In the momentum equations the pressure is assumed to be hydrostatic. The wave-induced driving force S_α in Eq. (10) is also of second order. By assuming that material derivatives of mean quantities are small, the full expression for S_α, given in Groeneweg (1999), can be simplified to:

$$S_\alpha=-\frac{1}{\rho}\frac{\partial\bar{\tau}_{j\alpha}^S}{\partial x_j}-\frac{\partial}{\partial x_j}\left(\overline{\tilde{u}_\alpha\tilde{u}_j}\right)+O\left(|\xi|^3\right) \tag{11.}$$

The second term of S_α is the well-known wave-induced stress. In the situation of waves without current this stress force is responsible for streaming. The first term denotes the gradient of the Stokes correction of the shear stress and denotes an imbalance term in the GLM equations. This term is wave-related and can be written entirely in terms of wave quantities, such as the corresponding shear stress component of the orbital motion. The relative importance of this term in the total wave-induced driving force S_α becomes more significant with increasing rotation. For regular non-breaking waves with a moderate current, both terms in Eq. (11) are of similar size (see Groeneweg, 1999). For breaking waves the first term will dominate over the second.

Vertically non-uniform distribution of wave-induced mass flux

In the GLM formulation the wave-induced mass flux is part of the depth-integrated GLM velocity, which is output of the model based on the flow equations (9) and

(10). By definition the relation between the GLM velocity and the Eulerian-mean velocity is the Stokes drift:

$$\overline{u} = \overline{u}^{L} - \overline{u}^{S} \tag{12.}$$

Consequently, part of the explanation of the wave-induced changes in the mean velocity profiles can be found in the (vertically non-uniform) Stokes drift.

Interpretation for Delft3D-FLOW. Although the flow equations (9) and (10) are not formulated in an Eulerian frame, the equations are of exactly the same form as the Eulerian-mean equations (1) and (2). Therefore, the implementation of the GLM equations is straightforward. Essential points that have to be considered carefully though are the boundary conditions at the bed and the free surface and at the boundaries of the domain under consideration.

Based on Groeneweg (1999) the following modifications were made to upgrade the Eulerian (wave-averaged) 3D flow model, Delft3D-FLOW, to a GLM-based model:

- The bed shear stress originates from Eulerian velocities (the bed “feels” Eulerian velocities). The near bed velocities are therefore corrected according to Eq. (12) to determine the bed shear stress.
- As the model now solves the shallow water equations for GLM velocities, the forcing on the model boundaries must be of the same type. At lateral model boundaries where waves are present, the GLM velocities must be defined (instead of Eulerian velocities).
- To obtain Eulerian flow velocities, the GLM velocities have to be corrected for the mass flux according to Eq. (12).

Furthermore, the turbulence model that relates the shear stresses with the strain rates is calibrated with Eulerian information. By modelling the turbulent motion as in the Eulerian settings, the interaction between the wave motion and the turbulent motion is neglected.

Incorporation of wave-induced turbulence

The wave effects in the turbulence model are accounted for by assuming an energy cascade in which the decay of organised wave energy is transferred to turbulent kinetic energy. The two main sources of wave energy decay that have been included are wave breaking and bottom friction due to the oscillatory wave motion in the bottom boundary layer.

In the case of breaking waves, there is a production of turbulent energy directly associated with the energy dissipation due to breaking (Deigaard et al., 1986). Wave energy dissipation due to bottom friction is also considered to produce turbulent kinetic energy. In the two-equation (k-ε) turbulence model of Delft3D-FLOW both sources are incorporated by introducing source terms in both the turbulent kinetic energy (k) equation and the turbulent kinetic energy dissipation (ε) equation. The contribution due to wave breaking is linearly distributed over a half wave height below the mean water surface (Figure 2). The contribution due to bottom friction is linearly distributed over the thickness of the wave boundary layer (Figure 2).

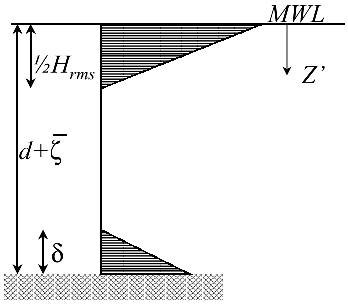

Figure 2. Vertical distribution of turbulent kinetic energy production.

This gives the following expressions for the turbulent kinetic energy distribution:

$$P_k(z`) = \frac{4D_w}{H_{rms}}\left(1 - \frac{2z`}{H_{rms}}\right) \quad \text{for} \quad z` \leq 1/2\, H_{rms} \tag{13.}$$

due to breaking waves, and:

$$P_k(z`) = \frac{2D_f}{\delta}\left(1 - \frac{d+\overline{\zeta}-z`}{\delta}\right) \quad \text{for} \quad d+\overline{\zeta}-\delta \leq z` \leq d+\overline{\zeta} \tag{14.}$$

due to wave energy decay in the bottom boundary layer. Here z' is the vertical coordinate with its origin in the (wave averaged) water level and positive downwards, D_w and D_f represent wave energy dissipation due to wave breaking and bottom friction, respectively. The source term, P_ε, in the ε-equation is coupled to P_k according to:

$$P_\varepsilon(z`) = c_{1\varepsilon}\frac{\varepsilon}{k}P_k(z`) \tag{15.}$$

where $c_{1\varepsilon}$ is a calibration constant ($c_{1\varepsilon}=1.44$).

Wave-induced driving forces

Streaming (a wave-induced current in the wave boundary layer directed in the wave propagation direction) is modelled as a time-averaged shear stress which results from the fact that the horizontal and vertical orbital velocities are not exactly 90° out of phase. It is based on the wave bottom dissipation (D_f) and is assumed to decrease linearly to zero across the wave boundary layer (Fredsøe and Deigaard, 1992):

$$\frac{\partial}{\partial x_j}\left(\overline{\tilde{u}\tilde{w}}\right) = -\frac{1}{\delta}\frac{D_f}{c} \qquad (16.)$$

where c is the phase velocity.

The dissipation due to bottom friction is written as:

$$D_f = \frac{1}{2\sqrt{\pi}}\rho f_w u_{orb}^3 \qquad (17.)$$

where u_{orb} is the orbital velocity near the bed based on the root mean square wave height and f_w is the friction factor according to Soulsby et al. (1993).

The additional shear stress due to streaming decreases linearly to zero across the wave boundary layer:

$$\tau_{str}(z`) = \frac{D_f}{c}\left(1 - \frac{d + \overline{\zeta} - z`}{\delta}\right) \quad \text{for} \quad d + \overline{\zeta} - \delta \leq z` \leq d + \overline{\zeta} \qquad (18.)$$

Wave forcing due to wave breaking is modelled as a shear stress at the water surface and is related to the wave dissipation (Svendsen, 1985 and Stive and Wind, 1986):

$$\tau_{br} = \frac{D_w}{c} \qquad (19.)$$

Comparison with Measurements

Two different types of experiments, in which the physical processes described above are thought to be important, were used for model validation. In the comparison the wave-related quantities were modelled separately and were used as input to determine the wave effects in the mean flow model. The first experiment (Klopman, 1994) involved non-breaking waves and their interaction with a steady current. The predicted streaming and vertically non-uniform mass flux distribution were compared with data from this experiment. In the second experiment (LIP11D, Arcilla et al., 1994) a typical surf zone was considered on proto-type scale. Data from this experiment was used to verify the forcing and enhanced turbulence due to wave breaking.

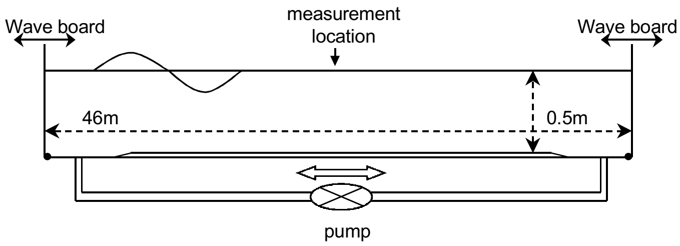

Figure 3. Schematic overview of experimental set-up in the Schelde flume.

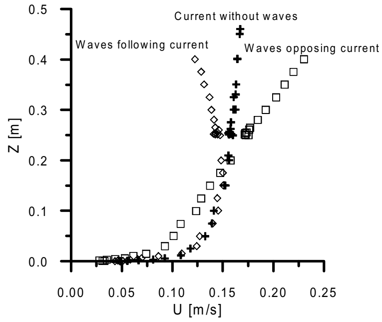

Figure 4. Results of Klopman (1994)

Klopman (1994) experiment. The Klopman (1994) experiment, conducted in a wave-current channel, investigated the combined motion of a current with mono-chromatic, bi-chromatic and random waves. Test series were performed for waves following and waves opposing the current, as well as for waves without a current and for a current without waves (see Figures 3 and 4). The three series with random waves were used in this study. No scaling was applied in the construction of the numerical model which therefore had the same dimensions as the Klopman experiment. The test series with currents only was used to derive the roughness value applied in the model.

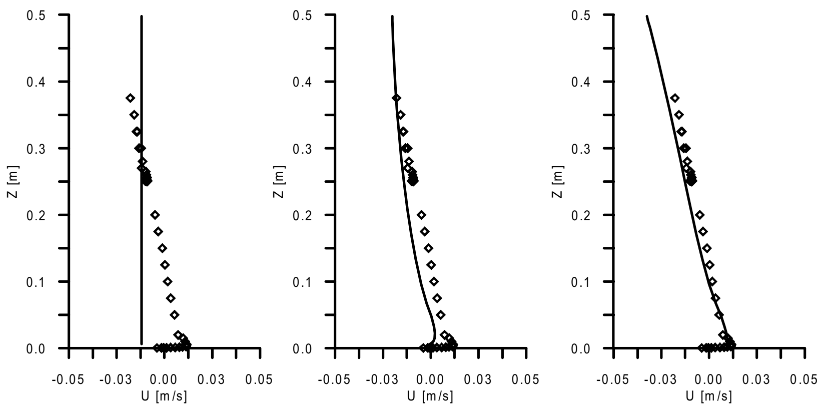

Figure 5. Comparison of model (solid) with measurements (symbols); left: uniform mass flux no streaming, middle: uniform mass flux with streaming included, right: non-uniform mass flux with streaming included.

In Figure 5 the model is compared with measurements for the case with waves only. The left graph shows the model results if a uniform mass flux is applied and streaming effects are excluded. Because the equations are solved for GLM velocities, which are corrected to Eulerian velocities at the bottom to determine the bottom shear stress, the wave motion induces no (wave-averaged) bottom shear stress. A significant improvement can already be seen in the middle graph when the streaming effect is included. In the graph on the right hand side the 2nd order analytical expression for the Stokes drift is used to convert the GLM velocities back to Eulerian velocities. The computed velocity profile now compares well with the measurements. In the lower part of the water column the correspondence is excellent. In the upper part some deviations can be observed. These are probably due to our relatively simple GLM model that does not include all terms.

In Figure 6, the cases with waves opposing (left graph) and following (right graph) the mean currents are shown. Qualitatively, the model shows the correct behaviour: for the opposing wave case the mean velocity profile shows a relatively linear increase towards the free surface, whereas the waves following the mean current results in a velocity profile which is very rounded. In the upper half of the water column the following waves have smaller (averaged) velocities compared with the opposing waves. It seems that the non-uniform mass flux distribution can partly explain this phenomenon. As with the no-current case (Figure 5) deviations are due to our relatively simple implementation of the wave-induced driving forces.

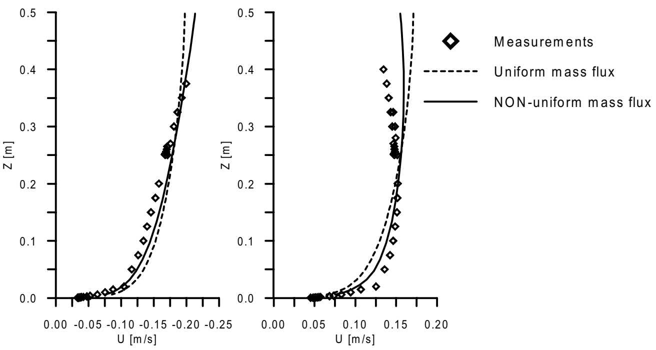

Figure 6. Comparison of model (solid) with measurements (symbols); left: waves opposing mean current and right: waves following mean current (in both graphs waves are travelling from right to left).

LIP11D experiments. In these experiments, carried out in the WL | Delft Hydraulics' Delta flume, detailed measurements of the hydrodynamics and sediment transports in surf zone conditions were made. The flume has a maximum length of 250 m. Using a water depth of 4.1 m, the length of the constructed bottom profile was approximately 180 m (Figure 7). Two cases were used in this study: Test 1A ($H_{m0}=0.9\ m$, $T_p=5\ s$) and Test 1B ($H_{m0}=1.4\ m$, $T_p=5\ s$).

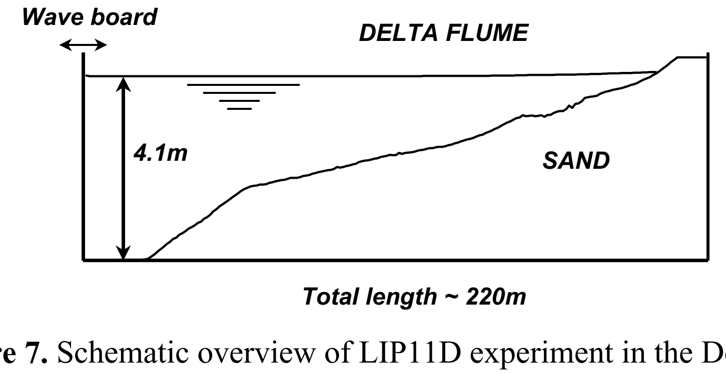

Figure 7. Schematic overview of LIP11D experiment in the Delta flume.

TEST 1A. In Figure 8 the wave height distribution and the bottom profile are shown. The vertical lines in the bottom profile indicate the locations at which velocity measurements have been taken (see Figure 9).

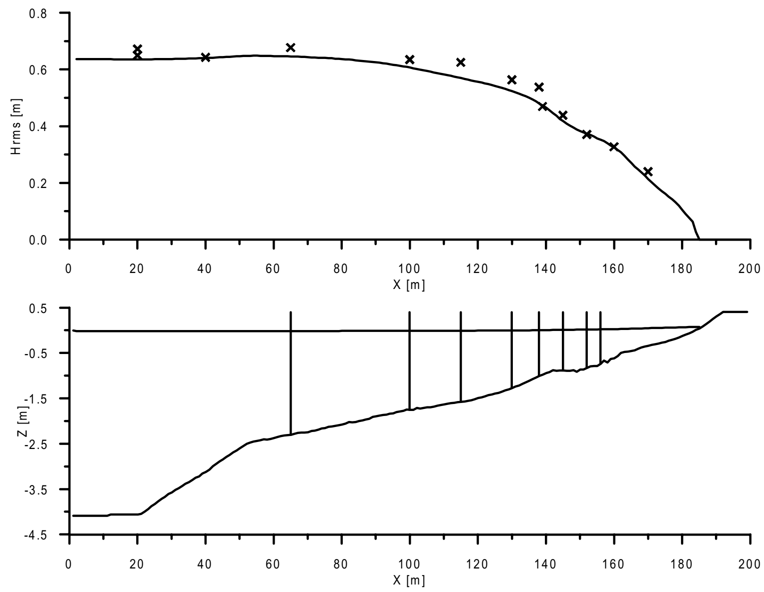

Figure 8. Wave height and bottom profile with locations of undertow measurements for Test 1A.

In Figure 9 the vertical cross-shore velocity profiles are shown. There is reasonable agreement with the measurements. At locations where there is less agreement (e.g. at *x=100*, *x=115* and *x=145*), predictions of the wave height gradients, which determine the dissipation that drives the flow model (Eq. 19), are relatively poor as well. It seems that the flow model gives an accurate description of the vertical flow structure if the correct wave forcing is applied.

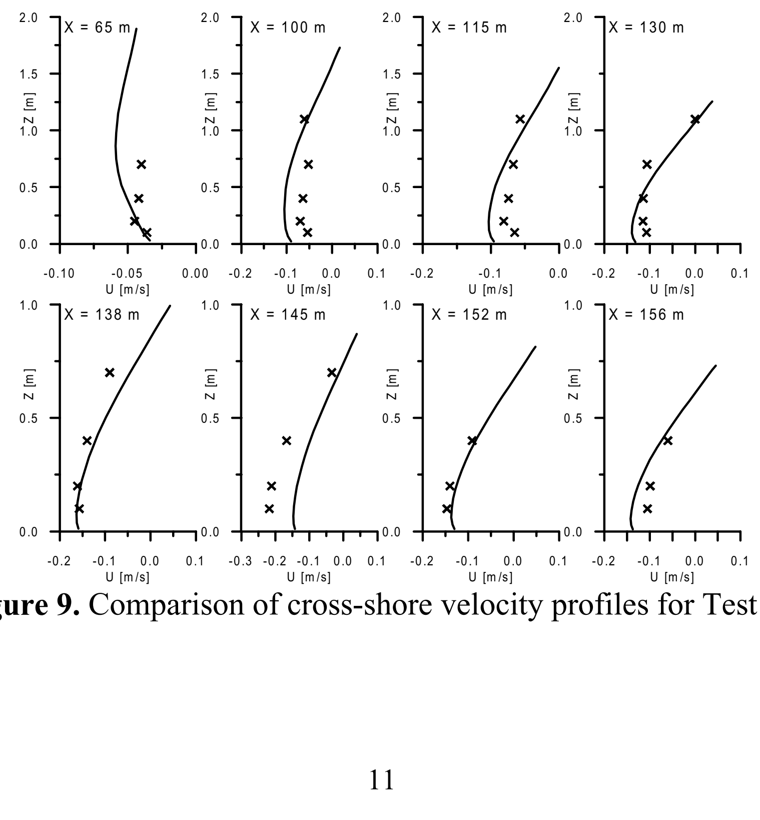

Figure 9. Comparison of cross-shore velocity profiles for Test 1A.

TEST 1B. In Figure 10 the wave height distribution and the bottom profile are shown. Again, the vertical lines in the bottom profile indicate the locations at which velocity measurements were taken. The wave height predictions for Test 1B show good agreement with the measurements. However, the wave height decay on top of the bar (at *x=138* m) is somewhat under-predicted.

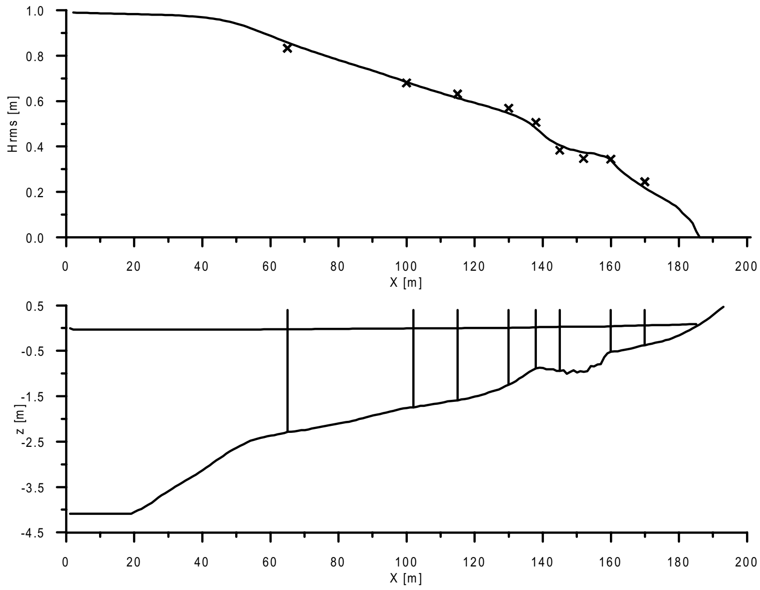

Figure 10. Wave height and bottom profile with locations of undertow measurements for Test 1B.

In Figure 11 there is generally good agreement with the measurements. However, on top of the bar (*x=138* m) and in the trough behind the bar (*x=145* m) agreement is poor. At both locations this is caused by incorrect wave forcing. The velocities on top

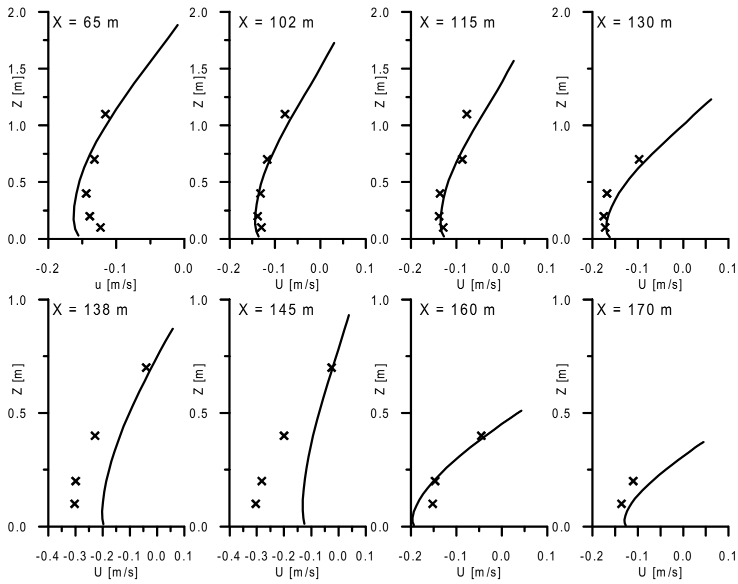

Figure 11. Comparison of cross-shore velocity profiles for Test 1B.

of the bar are under-estimated due to an under-prediction of the wave height decay at this location (see Figure 10). The under-prediction of the velocities in the trough ($x=145$ m) is caused by the absence of a roller model in the wave model. There is no persistence in the wave forcing in the trough area behind the bar, which results in an under-estimation of the velocities at this location.

For both cases the flow model is able to give an accurate description of the vertical flow structure, if the wave forcing is correct. This is an indication that the transfer of wave energy decay due to breaking to the turbulent motion is accounted for with sufficient accuracy.

Conclusions and Recommendations

The inclusion of turbulent kinetic energy sources due to wave dissipation (wave breaking and bottom friction) in the two equations turbulence (k-ε) model has yielded realistic results. The turbulence model predictions have not yet been compared with measurements directly. However, 3D suspended sediment transport simulations in which these terms were also included compared remarkably well with measurements (Lesser et al., 2000).

The inclusion of wave-induced streaming in the wave boundary layer was necessary to obtain correct velocity predictions in the Klopman experiment. This indicates that this phenomenon must be included in area models as it may be the significant driving force of the lower part of the water column at intermediate depths just seaward of the surf zone.

The GLM method has enabled us to include wave-induced mass flux in 2DH and 3D mean flow models in a natural way. Although the model has only been tested against laboratory experiments in this study (which essentially only requires a 2DV model), the model has successfully been applied in proto-type conditions in 2DH mode (Elias et al., 2000).

The comparison with measurements has shown that the Stokes drift forms part of the wave-induced changes in the mean flow profiles. However, we feel that the model can be improved further by including the vertically non-uniform wave-induced driving forces as given in Groeneweg (1999).

Finally, this paper has illustrated the potential of the GLM theory to significantly improve existing (Eulerian-based) numerical flow models at very little cost. With minor modifications any Eulerian-based 2DV, 2DH, Q3D or 3D mean current model can be re-formulated as a (simplified) GLM model.

Acknowledgements

The work has been supported by the Commission of the European Union, Directorate General for Science, Research and Development, in the SASME project under contract NO. MAS3 CT97-0081. This project was also partly funded by the Delft Cluster Project Coasts 03.01.03. The help of Mr. G. Lesser with the implementations in Delft3D-FLOW is greatly appreciated.

References

Andrews, D.G. and M.E. McIntyre (1978). An exact theory of nonlinear waves on a Lagrangian-mean flow, J. Fluid Mech., Vol. 89 (4), pp. 609-646.
Arcilla, A.S., J.A. Roelvink, B.A. O'Connor and J.A. Jimenez (1994). The Delta flume '93 experiment, Proc. Int. Coastal Dynamics Conference, UPC, Barcelona, pp. 488-502.
Bühler, O. and M.E. McIntyre (1978). On non-dissipative wave-mean interactions in the atmosphere or oceans, J. Fluid Mech., Vol. 354, pp. 301-343.
Deigaard, R., J. Fredsøe and I. Brøker Hedegaard (1986). Suspended sediment in the surf zone, J. of Waterway Port, Coastal and Ocean Eng., 112(1), pp. 115-128.
De Vriend, H.J. and N. Kitou (1990). Incorporation of wave effects in a 3D hydrostatic mean current model, Proc. 22nd Int. Conf. on Coastal Eng., Delft, The Netherlands, pp.1005-1018.
Elias, E.P.L., D.J.R. Walstra, J.A. Roelvink, M.J.F. Stive and M.D. Klein (2000). Hydrodynamic validation of Delft3D with measurements at Egmond, Proc. 27th Int. Conf. on Coastal Eng., Sydney, Australia.
Fredsøe, J. and R. Deigaard (1992). Mechanics of Coastal Sediment Transport. Advanced series on ocean engineering - Vol. 3, World Scientific Publishing.
Groeneweg, J. and G. Klopman (1998). Changes of the mean velocity profiles in the combined wave-current motion in a GLM formulation, J. Fluid Mech., Vol. 370, pp. 271-296.
Groeneweg, J. (1999). Wave-current interactions in a generalized Lagrangian mean formulation, PhD thesis, Delft University of Technology, Delft.
Klopman, G. (1994). Vertical structure of the flow due to waves and currents: Laser-Doppler flow measurements for waves following or opposing a current, Delft Hydraulics, Report no. H840.32, Part 2.
Lesser, G., J.A. Roelvink and J. van Kester (2000). Online Sediment Transport Within Delft3D-FLOW, WL | Delft Hydraulics, Report no. Z2396/Z2899.
Phillips, O.M. (1977). The dynamics of the upper ocean, Cambridge Univ. Press.
Soulsby, R.L., L. Hamm, G. Klopman, D. Myrhaug, R.R. Simons and G.P. Thomas (1993). Wave-current interaction within and outside the bottom boundary layer, Coastal Eng., 21, pp. 41-69.
Stive, M.J.F. and H.G. Wind (1986). Cross-shore mean flow in the surf zone, Coastal Eng., 10, pp. 235-340.
Svendsen, I.A. (1985). On the formulation of the cross-shore wave-current problem, Proc. Workshop "European Coastal Zones". Athens, pp. 1.1-1.9.